Heliyon 10 (2024) e28144

Contents lists available at ScienceDirect

Heliyon

journal homepage: www.cell.com/heliyon

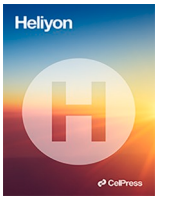

Research article

Characterization of modified titanium surfaces by anodisation and immersion tests

Dener Pedro da Silva Palma, Giovana Pedroso Silva, Fernanda Mathidios Zago, Eduardo Norberto Codaro, Heloisa Andréa Acciari *

São Paulo State University (Unesp), School of Engineering and Sciences, Department of Chemistry and Energy, Guaratinguetá, SP, 12516-410, Brazil

ARTICLE INFO

Keywords:
Anodisation
TiO_2 compact films
TiO_2 nanoporous films
Current-time transients
Hydrophilic properties

ABSTRACT

This paper explores the features of both nanoporous and compact TiO_2 films formed by titanium anodisation in two experimental conditions, given that they have completely different morphologies and properties than those found by our previous studies. After anodisation, samples have been subjected for 20 days to immersion tests in different media (H_2O, H_3PO_4, and KOH). Surface morphology, phase composition and wettability of anodised films were investigated using FESEM, FTIR, Raman spectroscopy, contact angle measurements and XPS, and the hydrophilicity of modified surfaces was investigated by immersion tests. Nanoporous films exhibited hydrophobic surfaces, but contact angle values gradually decreased after immersing films in H_2O, H_3PO_4 and KOH media, respectively. However, compact films produced superhydrophilic surfaces, both before and after immersion tests, with the exception of immersing the film in a H_3PO_4 medium due to film removal by acid attack. As for compact films, an unusual morphology revealed by the presence of cone-shaped particles might be responsible for the adsorption of –OH groups arranged so as to favour anatase phase formation.

1. Introduction

Recent research on titanium anodisation has focused on coupling two or more technologies to modify the characteristics and properties of anodic films. The morphology of TiO_2 films formed by anodic oxidation depends on a set of variables, such as the effects produced based on the number of steps in anodisation tests, type of organic solvent, or concentration of fluoride ions in the electrolyte, in addition to other extensively studied parameters, such as potential, current and anodisation time [1–4].

Pishkar et al. (2018) improved the structural order of produced nanotubes using a two-step anodisation method. They evidenced that nanotubes produced after the first anodisation step showed a less organized structure, while those produced by removing the film after the first step, followed by anodisation, presented a more orderly and compact hexagonal structures [5].

Wang et al. (2019) micro-milled a titanium surface prior to anodisation in order to produce a hierarchical surface pattern composed of a nano- and micro-textured layer on the same surface. These authors achieved more significant results regarding hydrophilic properties and cellular response due to the fact that this new surface has much greater roughness than pure titanium and anodised titanium surfaces, even without undergoing pre-treatment [6].

Niu et al. (2020) reported a novel, simple, reproducible and low-cost strategy for anodic TiO_2 film formation on titanium substrates.

* Corresponding author.
E-mail address: heloisa.acciari@unesp.br (H.A. Acciari).

https://doi.org/10.1016/j.heliyon.2024.e28144
Received 8 November 2023; Received in revised form 4 March 2024; Accepted 12 March 2024
Available online 20 March 2024

They have already observed that nanotubes can be converted into crystalline TiO_2 by immersion in H_3PO_4 medium, and that this new hierarchical pattern is similar to that of nanopetals. It is worth mentioning that all samples submitted to immersion tests showed rutile peaks in accordance with XRD patterns in their study [7]. In a similar work, samples immersed for over a day in H_3PO_4 medium exhibited diffraction peaks capable of being indexed to the rutile phase and, therefore, they found that this process is also capable of inducing film crystallization. These authors also report that a detailed mechanism of phase transformation has not been elucidated yet, although they suggested that it might be related to the fact that H_3PO_4 medium is able to dissolve TiO_2 (compared to pure H_2O) [8].

Yang et al. (2019) planned a sequence of three anodisation steps, in which nanotubes were produced during the first one, while a compact oxide layer was formed in the second one due to differences in electrolyte compositions. During the third step, a new layer of nanotubes was formed due to its experimental conditions being the same as those selected for the first one. These authors observed that, after the third step, both the length and diameter of formed nanotubes were greater than those detected in the first step. In addition, current-time curves were quite different in the first and third anodisation tests, although film morphology can be explained by nanotube growth in both cases [9].

Zhang et al. (2019) carried out sequential multi-stage galvanostatic anodisation tests with no intermediate operation between each step, i.e. the anodisation test of a following step having started right after the preceding one. In all steps, they observed that peak and stabilization voltages gradually decreased as fluorine ion concentration increased. Also, the diameter and length of nanotubes produced by three-step anodisation were greater than those found for the initially anodised nanotubes. Interestingly enough, they also found a surprisingly organized arrangement of nanotubes than those produced by single-step anodisation [10].

Xu and Jiang (2020) produced TiO_2 nanotubes through two-step anodisation on a titanium alloy surface. After the first anodisation step, samples were placed in an ultrasonic bath in order to supposedly remove the formed film, and then a second step was performed under the same anodisation conditions as in the first one. A nanotubular porous structure was observed after the first anodisation, and an oxide layer formed in the first step could not be thoroughly removed. Nanopores formed after the second anodisation step had significantly larger diameters, thus allowing us to clearly distinguish nanopores formed both in the first and second anodisation steps [11].

Ossowska et al., 2021 produced a dual-structure hybrid oxide film on the surface of Ti–13Nb–13Zr alloy by coupling thermal oxidation and anodic oxidation so as to improve corrosion resistance and biocompatibility. The film consisted of a crystalline oxide layer obtained from thermal oxidation and a hydrophilic and bioactive nanotubular layer with the purpose of producing a significant impact on bone-implant integration processes [12].

Given the studies reported above, it is worth emphasising that some make use of coupled tests which are simple and low-cost strategies. They are also quite promising, as they not only lead to a crystallization process, but to modifications in film morphology. Furthermore, there is a numerous amount of correlated works in which different techniques were coupled in order to obtain a new surface for optimal performance titanium implants [13–15]. In this context, this study aims to further explore this topic by coupling anodisation and immersion tests and investigate the resulting changes in hydrophilic characteristics and properties of films. The main theoretical sources considered to support such an investigation were grounded in works proposed by Wu et al. (2019) and Niu et al. (2020), as aforementioned [7,8], which are based on water-assisted crystallization of films. These authors consider that the ability of H_3PO_4 to dissolve TiO_2 (compared to pure water) and the presence of PO_4^{3-} ions play a crucial role in this process. Given that these results were rather surprising, we decided to carry out some tests by increasing immersion time, also in addition to introducing a KOH solution for comparison purposes, which could affect the wettability of films, as it provides -OH^- ions.

2. Material and methods

2.1. Sample preparation

Grade 4 Ti disks (ASTM F67) with 12 mm in diameter and 3 mm in thickness were used as metallic substrates in anodisation tests. Titanium samples were manually polished using abrasive silicon carbide (SiC) sandpaper having different granulations (from 220 to 3000 mesh). Final polishing was performed using 0.02 μm colloidal silica suspension and 5% oxalic acid solution in a polishing machine. Then, samples were placed in a beaker containing deionized water and taken to an ultrasonic bath for a 15-min cleaning cycle. Polished samples were immersed for 15 s in a chemical polishing solution composed of $HF + HNO_3 + H_2O$ (1:1:2 vol ratio), which were then rewashed ultrasonically using deionized water and air-dried afterwards.

2.2. Anodisation

The experimental setup used in anodisation tests consisted of a direct current source (Keysight E3643A), an ammeter (Micro-Química MQI-V) and an electrolytic cell, all connected in series. An ammeter converts signals provided by the source and arranges them via an output in mA/V directly to a potentiostat (Metrohm – Autolab PGSTAT 302 N) to record a voltage-time curve using the software Nova 2.1. As for its conversion into current data, 10 mA/V was considered for all tests based on the instrument scale background (Ammeter).

Anodisation tests were carried out in two experimental conditions selected to produce anodic films with different morphologies, as stated in some of our previous works [16,17]. The first tests were conducted at 50 V for 15 min using an ethylene glycol-based electrolyte with 0.5 wt% of NH_4F and 10 vol% of deionized H_2O. The second test was performed at 30 V for 6 h using a 0.25 M H_3PO_4 medium as electrolyte. In both experiments, a graphite sheet was used as cathode.

2.3. Immersion tests

After anodisation, a sample from each group has been immersed for 20 days in different media (deionized H_2O, H_3PO_4 10 wt% and 0.1 M KOH medium) using six glass beakers sealed with a plastic film kept at room temperature.

2.4. Surface characterization

Field Emission Scanning Electron Microscopy – FESEM (JEOL, JSM-7500F) was used to characterize the morphology of anodic films. Phase identification was performed using a Raman spectrometer and argon laser excitation at 532.2 nm and room temperature (Horiba Scientific T64000). Contact angle of deionized water was measured at room temperature using an angle-measuring instrument (ramé-hart instrument co.). Measurements were taken in different places on the surfaces of each sample, and mean values were calculated for each modified surface. Fourier-transform Infrared Spectroscopy - FTIR was used to identify functional groups in the molecular structures of samples. Characteristic absorption bands were evaluated by Attenuated Total Reflection (ATR), and 10 scans were taken to obtain each spectrum from 4000 to 650 cm^{-1} (PerkinElmer Spectrum 100 Spectrometer). XPS analysis was performed using a UNI-SPECS UHV System spectrometer at pressures of less than 5×10^{-7} Pa. The Al Kα line was used ($h\nu = 1254.6$ eV) as ionization source and the analyser pass energy was set to 10 eV. Shirley's method was used to subtract the inelastic noise of high-resolution C 1s, O 1s and Ti 2p spectra. Composition was measured based on the atomic percentage of surface layer (<5 nm) and found by relative proportions of areas of spectra corrected by Scofield's atomic sensitivity factors, whose accuracy was ±5%. Spectra were deconvoluted using a Voigtian-type function with Gaussian (70%) and Lorentzian (30%) combinations. Full width at half maximum (FWHM) varied between 1.2 and 2.1 eV, and the position of peaks was determined with an accuracy of ±0.1 eV.

3. Results and discussion

Fig. 1 shows transients related to anodisation tests carried out herein in two experimental conditions. The curves depicted in Fig. 1 (a, b) reveal an initial increase in current density followed by a sharp drop, possibly due to oxidation and dissolution of titanium and an oxide layer formed afterwards. It is assumed that the oxide layer has a compact structure in this initial stage. A subsequent current density increase might indicate the beginning of a new stage in layer growth kinetics, resulting in a porous structure which is probably due to the formation of oxygen gas bubbles thereof. At the final stage, current density decreases to its lowest value, thus revealing a steady state between layer formation and dissolution. It is worth mentioning that current density values were significantly lower when anodisation was performed in H_3PO_4 medium (Fig. 1(b)). In addition, a slight variation in current density values suggests a gradual titanium surface coating and the formation of a more compact layer which stops growing the moment current density reaches its steady state.

It is noteworthy that the same event, denoted by another increase in current density, is observed at different time intervals by comparing the graphs shown in Fig. 1(a) and (b), which might be due to the electrolyte nature. Several authors have focused on this topic aiming to determine how the electrolyte affects film growth kinetics and its morphology whilst producing porous or compact films. Sivaprakash and Narayanan (2020) investigated dimensional aspects of TiO_2 nanotubes produced in electrolytes containing ethylene glycol as solvent by varying the amount of water by 5 and 10% in volume. They found that the length of nanotubes increased as water content rose [18]. Liao et al. (2017) produced both compact anodic titanium oxide and nanotube films from mixed electrolytes, and found differences in galvanostatic anodisation curves attributed to the presence of an ionic current associated with compact oxide growth, in addition to an electronic one related to oxygen bubbles responsible for the formation of pores on the film [19]. Qin et al. (2021) investigated the effect of electrolyte viscosity on the sizes of TiO_2 nanotubes and water content varied from 0.5 to 4 wt% using both ethylene glycol and glycerol solvents. These authors found that pore growth started at different stages of current

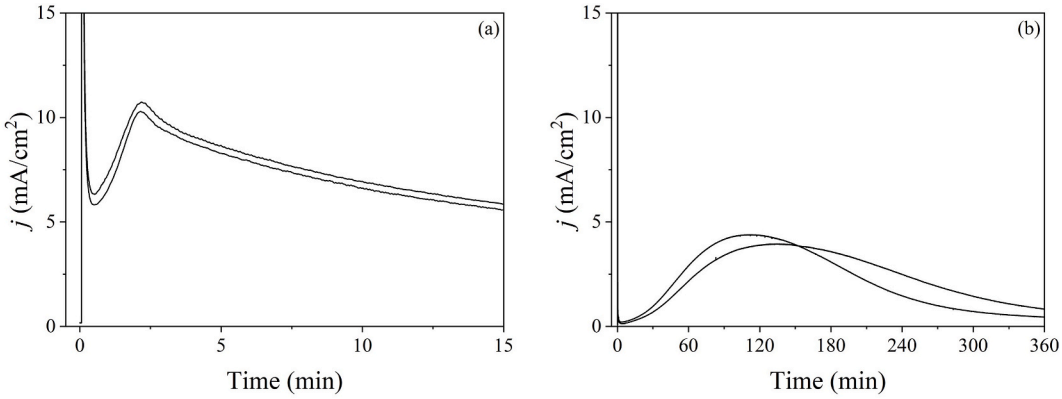

Fig. 1. Current – time curves related to anodisation tests in: (a) ethylene glycol electrolyte; (b) H_3PO_4 electrolyte. Duplicate tests in each experimental condition.

transients by changing potential from 3 V to 5 V. They also observed that the greater the concentration of fluoride ions in the electrolyte is, the faster pores started to grow, probably on account of the fact that viscosity coefficient is rather low in aqueous media, and ions generated by oxidation and hydrolysis of titanium diffuse more rapidly and can, therefore, corrode oxide films more rapidly. Furthermore, a higher concentration of these ions on the inner walls of nanotubes would lead to an increase in their diameters. However, viscosity in glycerol is so intense that it takes longer for fluoride ions to reach the base of pores, and there should be inner wall dissolution at a higher concentration of H^+ ions the moment these ions finally reach it so as to form larger nanotubes [20]. Zhou et al. (2020) compared different current transients and morphologies of films produced in different electrolytes. These authors report that nanotubes were only formed in an electrolyte containing ethylene glycol, while a dense TiO_2 film was obtained from the ethanol electrolyte. The authors also observed that both an ionic current, typically dominant at the beginning of anodisation, and an electronic current, usually generated in the second stage and characterized by the formation of oxygen bubbles, were considerably lower whilst performing anodisation in an ethanol electrolyte if compared to those in an ethylene glycol electrolyte [21].

3.1. Field Emission Scanning Electron Microscopy – FESEM

Fig. 2 shows FESEM images of titanium surfaces after anodisation in ethylene glycol at 50 V, Fig. 2(a), in addition to those produced after the immersion tests, Fig. 2(b–d). After anodisation, a porous structure was produced, whose pore diameters range from 32 to 102 nm. The formation of small valleys connecting the pores to one another can also be clearly observed. The immersion test in H_3PO_4 medium should have partially removed the porous layer, providing the substrate surface with a lamellar texture, whereas for the samples immersed in either H_2O or KOH media, there was no significant change in the original film morphology.

Fig. 3 shows FESEM images of titanium surfaces after anodisation in 0.25 M H_3PO_4 medium, Fig. 3(a), and also those obtained after immersion tests, Fig. 3(b–d). The morphology of films in this experimental condition has already been described in our previous works [16,17], i.e. it is characterized by the presence of cone-shaped particles (light grey area) arranged on an amorphous and compact layer (dark grey area). Once again, no significant morphology changes were observed after 20 days in deionized H_2O or KOH media. On the other hand, it seems as though part of the film was removed by acid attack after immersion in H_3PO_4 medium.

Such significant variations in the morphologies of films, both before and after immersion tests, were not observed, as those found by Wu et al. (2019) and Niu et al. (2020) [7,8] in which nanotubes were converted into flower-like structures. The reason for such a

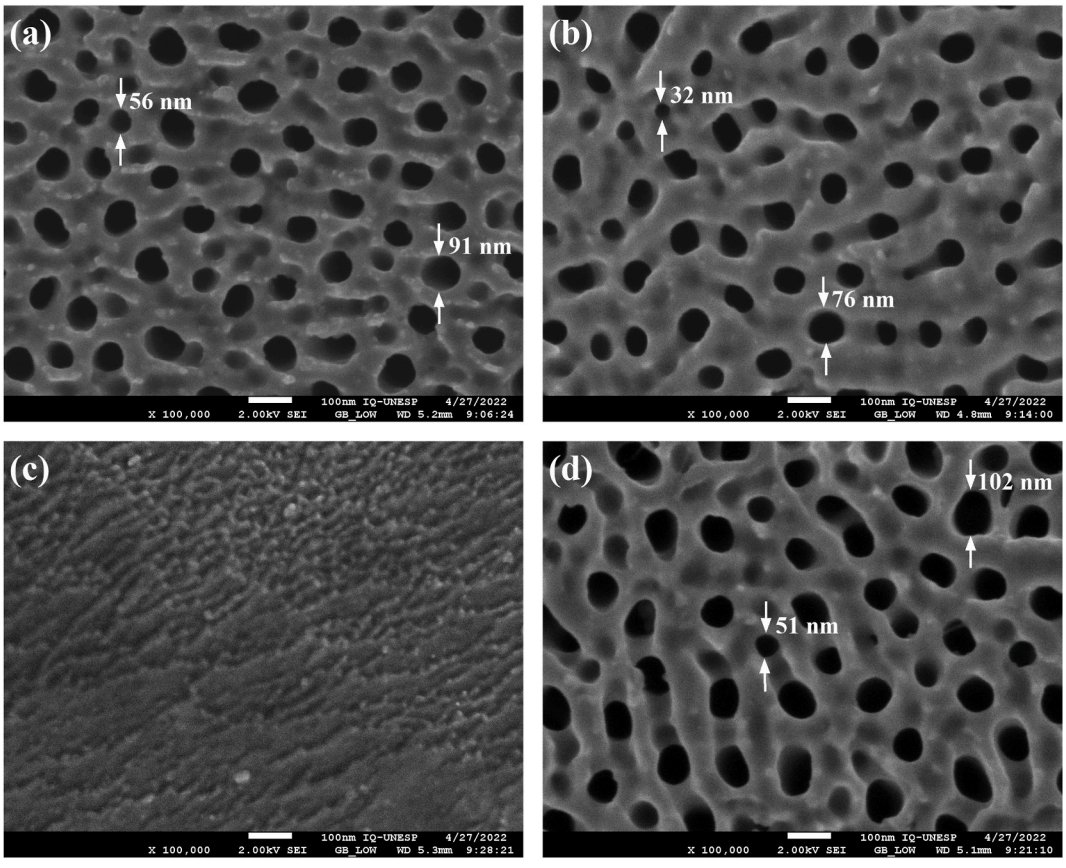

Fig. 2. Titanium surfaces FESEM images after anodisation at 50 V for 1 h in ethylene glycol electrolyte: before immersion tests (a); after 20 days of immersion in deionized H_2O (b), in H_3PO_4 10 wt% (c); and in 0.1 M KOH solution (d).

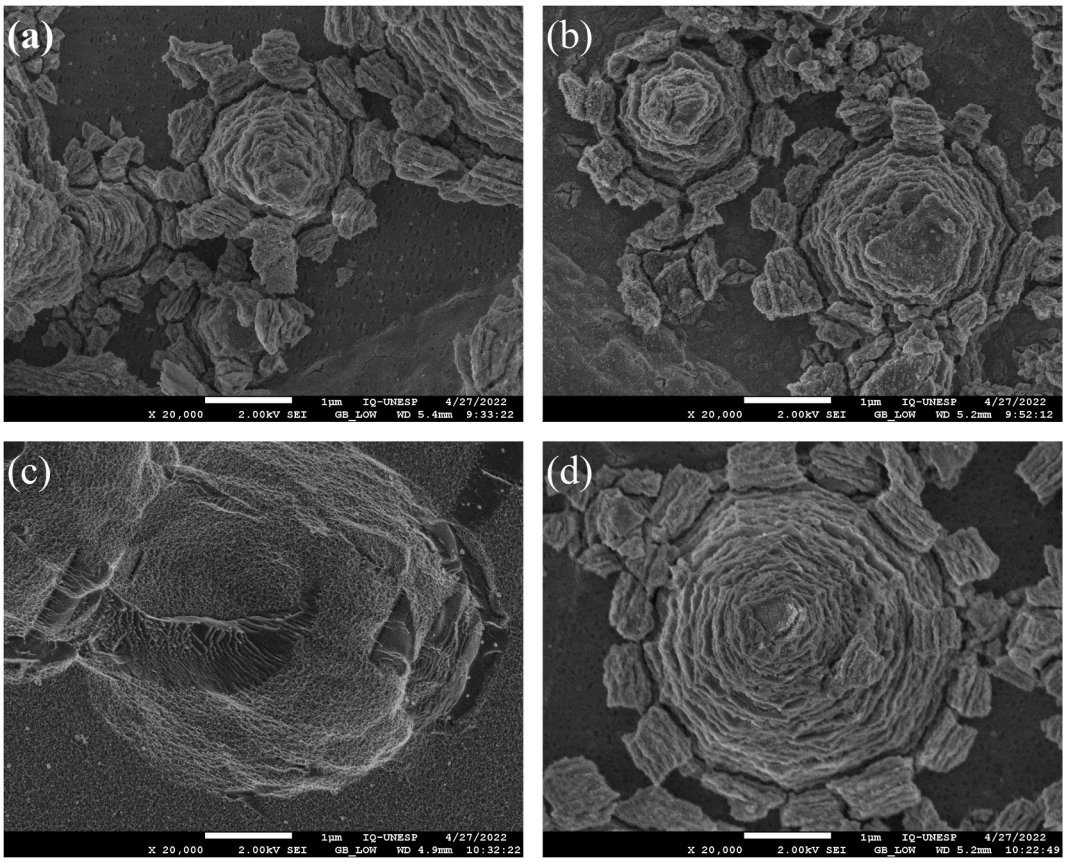

Fig. 3. FESEM images obtained for titanium surfaces after anodisation at 30 V during 6 h in 0.25 M H_3PO_4 solution: before immersion tests (a); after 20 days of immersion in deionized H_2O (b), in H_3PO_4 10 wt% (c); and in 0.1 M KOH solution (d).

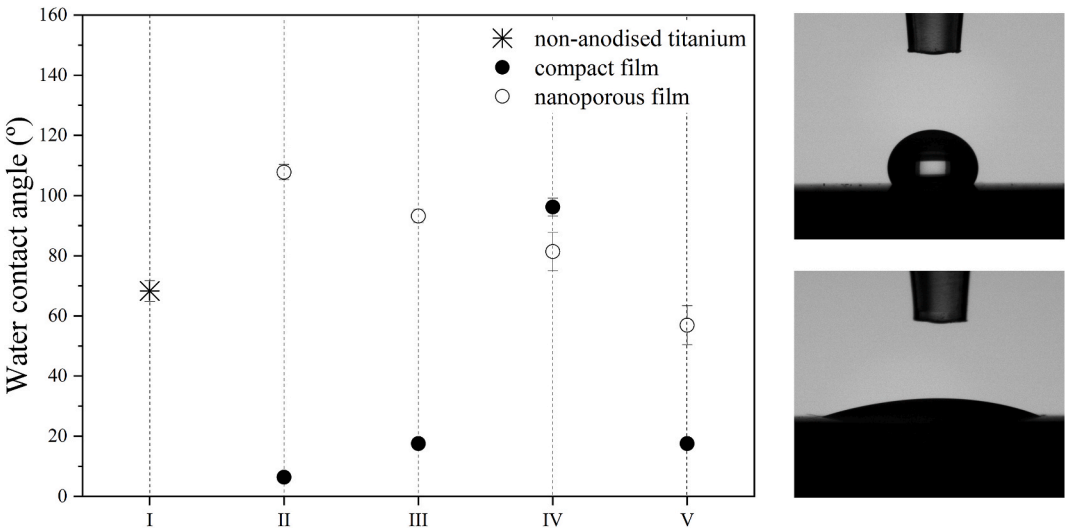

Fig. 4. Contact angle measurements of modified surfaces: non-anodised titanium (I); after anodisation (II); after immersion in deionized H_2O (III), H_3PO_4 solution (IV), and KOH solution (V). Representative images of water droplets on film surfaces during measurements (the highest contact angle value is at the top and the lowest at the bottom).

divergence might be due to the fact that these authors investigated immersion tests of nanotube films, instead of nanoporous or compact ones, thus the dimensions of these particular pore shapes, such as diameter/length ratio, might play an important role in this conversion mechanism.

3.2. Contact angle measurements

The contact angle of polished titanium surface was 68.3° with no anodisation treatment, as in Fig. 4, which is in good agreement with results achieved by other authors [8,22]. The anodisation process generally produces hydrophilic surfaces due to the porous nature of formed films. However, the nanoporous film surface is hydrophobic according to its contact angle, whereas films characterized by the presence of cone-shaped particles are superhydrophilic.

Hydrophobic surfaces can be explained by the Cassie-Baxter effect which is exerted the moment atmospheric air trapped within pores provides resistance to the penetration of water into them. However, such an effect tends to reverse over time as trapped air is released and water is absorbed by the capillarity of nanopores [23].

Results from immersion tests reveal a decrease in contact angle values for nanoporous films according to different immersion media used herein. Superhydrophilic surfaces were produced when samples were anodised in the aqueous electrolyte and also after immersion in H_2O or KOH media, in addition to a significant reduction in contact angles from 68.3° (I) to 6.4° (II), 17.5° (III) and 13.9° (V), with the exception of sample IV whose contact angle is 96.2°, i.e. a hydrophobic surface, most likely due to the fact that the acid solution had partially dissolved cone-shaped crystalline particles. Aeimbhu (2018) reported that increasing temperature during heat treatments affects the wettability of TiO_2 films. Moreover, results show that contact angle has decreased from 75.1° to approximately 15°, thus making the surface more hydrophilic, possibly due to the formation of crystalline phases in the initial amorphous film [24].

3.3. Fourier-transform Infrared Spectroscopy (FT-IR)

FT-IR spectra of surfaces after anodisation tests in both experimental conditions investigated herein are shown in Fig. 5. The

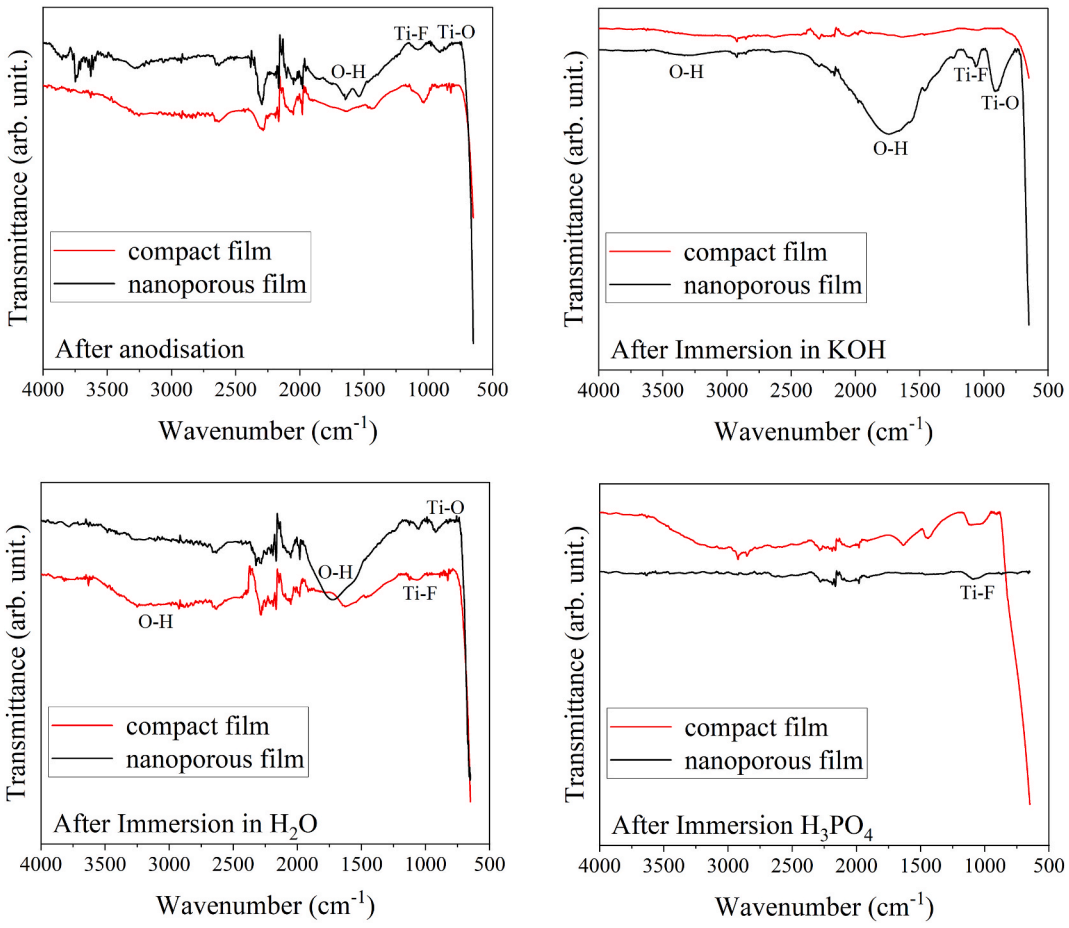

Fig. 5. FTIR spectra obtained for modified surfaces: after anodisation (II); after immersion in deionized H_2O (III), H_3PO_4 medium (IV), and KOH medium (V).

presence of a peak near 750 cm^{-1} might be related to the formation of Ti–O bonds of titanium dioxide films [23,25–27]. The absorption peak near 1100 cm^{-1} might be ascribed to the F–Ti bond vibration [27]. The band around 1700 cm^{-1} is assigned to the bending vibration of O–H bond [25,28] and might be associated to humidity in air atmosphere possibly due to the absorption of water molecules [23]. The band at around 3400 cm^{-1} is assigned to the vibration of hydroxyl groups [26,28,29]. A comparison of spectra suggests that the determining factor in the lowest contact angle values (Fig. 4) must be related to the anodic film morphology, rather than the presence of $-OH^-$ groups on modified surfaces, considering that bands around 1700 cm^{-1}, related to water absorption, were more prominent for nanoporous films (originally amorphous), with the exception of the sample IV (after immersion in H_3PO_4, which must have led to film dissolution).

3.4. Raman spectroscopy

Raman spectroscopy of anodic oxide films was performed on cone-shaped particles shown in the light grey area of Fig. 3, and bands at around 144, 396, 516 and 634 cm^{-1} were found and shown in Fig. 6. The band at around 144 cm^{-1} is assigned to the long-range order of anatase phase, whereas the remaining bands are related to its short-range order. These results reveal that cone-shaped particles refer to areas of crystalline nuclei in the amorphous film. On the other hand, no Raman peaks were found in the compact layer area around cone-shaped particles, nor on nanoporous films, which are generally associated with amorphous or nanocrystalline films. There is also no evidence of bands for sample IV for the compact film, most likely due to partial film removal after immersion in the acid solution, which supports the hypothesis that the presence of cone-shaped crystalline particles refers to the anatase phase.

3.5. XPS analysis

The atomic concentration (at. %) of surface layer elements (<5 nm) of samples was obtained from high-resolution spectra (Fig. 7). N, F, and P are residues of the electrolyte used (Ca contamination by manually handling samples). Samples have a high concentration of carbon on their surfaces (hydrocarbon contamination due to the aging of samples). Sample immersion in KOH medium enlarges the contaminating layer, thus attenuating the titanium signal.

3.6. Local chemical structure

3.6.1. O 1s

The main component of oxygen spectra at 530.0 eV is due to O–Ti bonds of TiO_2. Surface hydroxyl groups (531.5 eV) and O=C groups have high binding energy. Other oxidized carbon groups O–C and O–C=O appear at 532.6 eV and 533.5 eV, respectively. The intensity of oxygenated groups increases for samples after immersion in KOH medium, as in Fig. 8.

3.6.2. C 1s

The main component at 284.9 eV is on account of hydrocarbons (C–H) from surface contamination, as it contains oxygenated alcohol/ether O–C, carbonyl C=O and carboxyl O–C=O groups at 286.5 eV, 287.4 and 288.8 eV, respectively (Fig. 8). No significant changes were observed in samples anodised at 50 V and immersed in KOH medium, whereas the intensity of C–O and C=O groups increased for samples at 30 V.

3.6.3. Ti $2p_{3/2}$

All titanium spectra of the Ti $2p_{3/2}$ and Ti $2p_{1/2}$ spin-orbit pair were fitted with a component at 458.7 eV (Ti $2p_{3/2}$) associated with the TiO_2 phase. Full width at half-maximum (FWHM) of 1.5 eV reveals no contribution from another phase (Ti^{3+} with binding energy

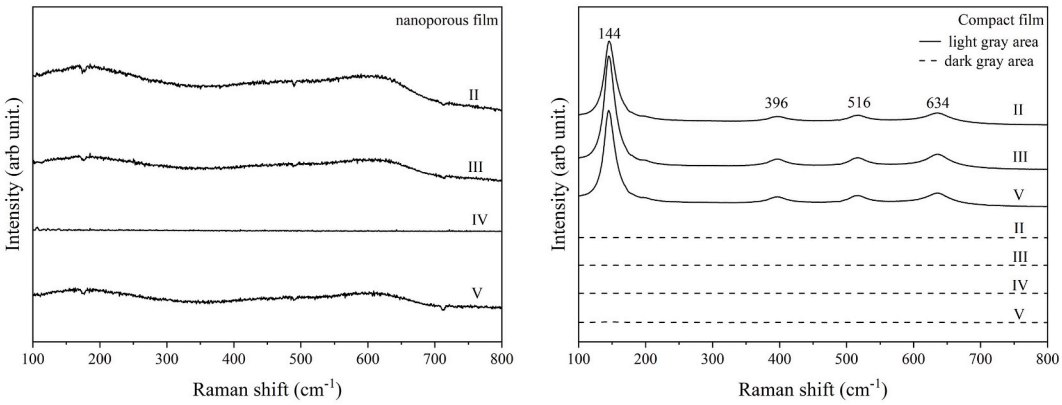

Fig. 6. Raman spectra obtained for titanium modified surfaces: after anodisation (II); after immersion in deionized H_2O (III), H_3PO_4 medium (IV), and KOH medium (V).

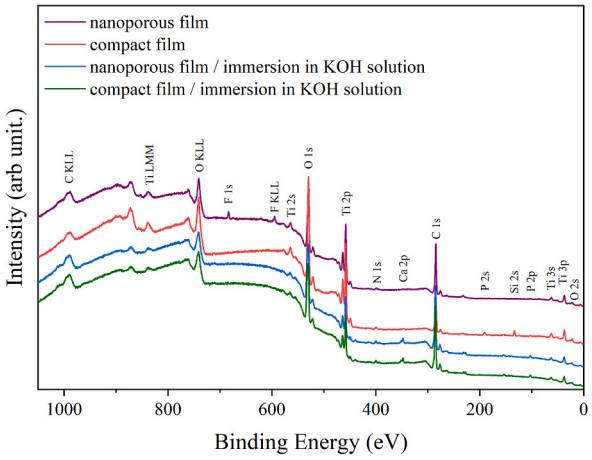

Fig. 7. XPS survey spectra of nanoporous and compact films before and after immersion in KOH medium.

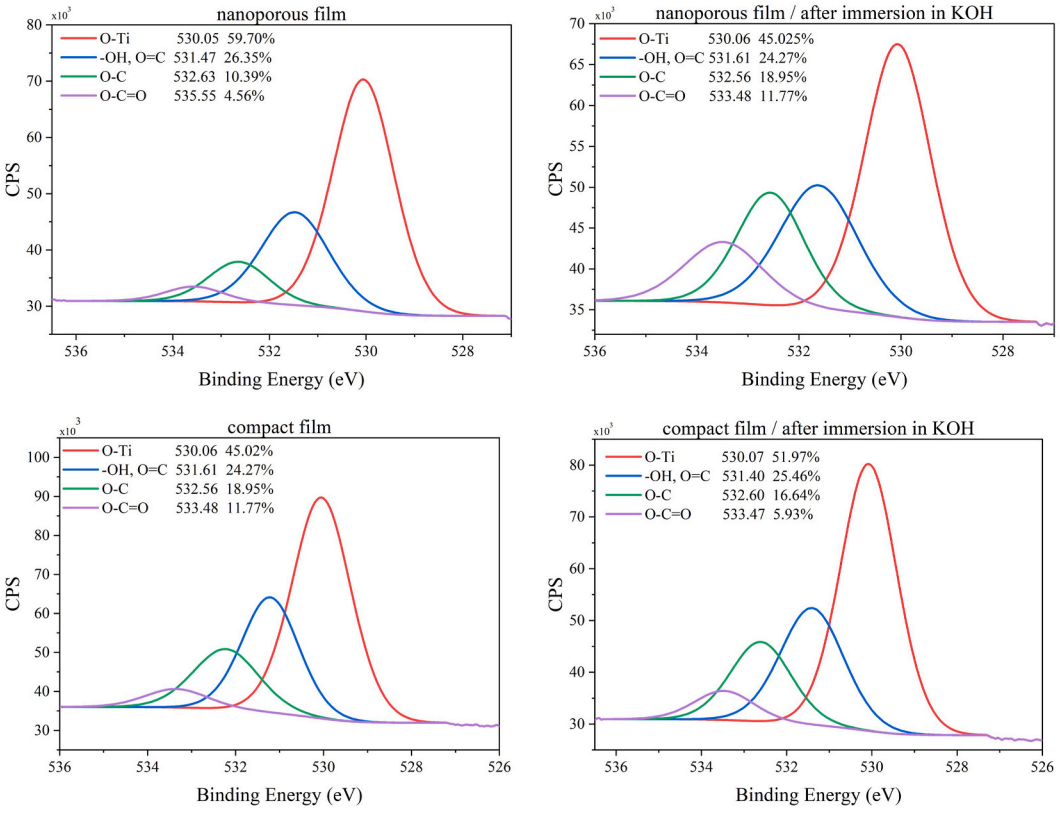

Fig. 8. Deconvoluted XPS peaks spectrum of nanoporous and compact films before and after immersion in KOH medium.

1.0–1.5 eV below that of TiO_2). No significant changes are observed in samples immersed in KOH medium.

3.7. Comparative remarks

Immersion tests are based on the water-assisted crystallization of amorphous films. According to previous studies [30,31], it is assumed that TiO_6 octahedra, randomly arranged in the amorphous film structure, are reorganized by sharing their vertex, initially through absorbing water molecules and then forming a bridge between the hydroxyl groups on its surface through lone pair of

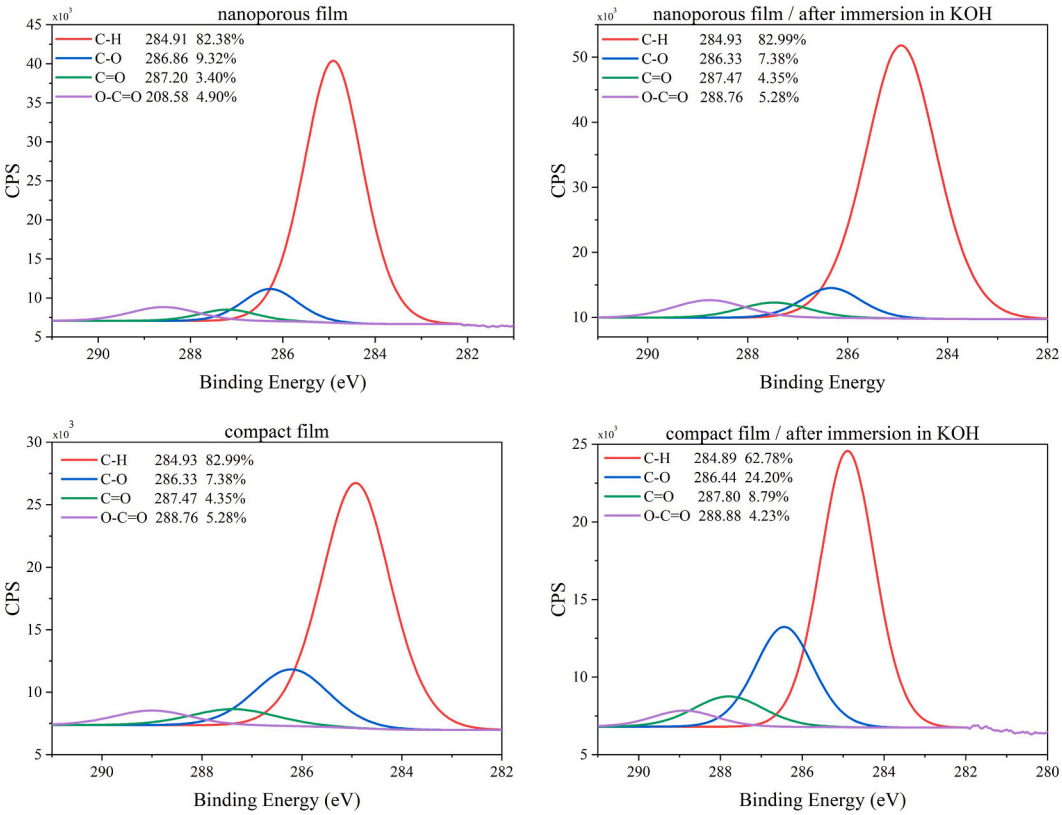

Fig. 8. (*continued*).

electrons in oxygen. In a subsequent step, the $Ti(OH)_6^{2-}$complex must be dehydrated by eliminating two water molecules and one oxygen atom, thus resulting in the sharing of these octahedra orientated towards the formation of a unit cell the TiO_2 anatase afterwards. In a few words, the TiO_6 octahedra in the amorphous TiO_2 film dissolve in water, and probably forms complex ions $Ti(OH)_6^{2-}$ capable of spontaneously recrystallizing and precipitating in situ as crystalline TiO_2, as in Eqs. (1) and (2) [32].

$$TiO_{2(amorphous)} + 4H_2O \rightarrow Ti(OH)_6^{2-} + 2H^+ \quad (1)$$

$$Ti(OH)_6^{2-} + 2H^+ \rightarrow TiO_{2(crystalline)} + 4H_2O \quad (2)$$

As this phenomenon is promoted by the presence of hydroxyl groups on the surface, we conducted a more extensive study by adding the KOH solution in the tests, given that it is a medium able to provide hydroxyl ions, OH^-, although no significant differences were found in experimental results compared to using the H_2O and KOH solution as immersion media.

4. Conclusion

A nanoporous film was produced using an ethylene glycol electrolyte and a compact film was obtained from an acidic aqueous electrolyte. Changes in medium viscosity and pH have led to different profiles of current transients recorded during anodisation tests, and consequent differences were detected in the respective morphologies of films obtained through anodisation. The nanoporous film consisted of a hydrophobic surface, while the compact film had a superhydrophilic surface. Such a high degree of organization in the formation of cone-shaped particles not only relies on anodisation parameters, but also on mechanical and chemical polishing steps prior to it. Such an unusual morphology might be responsible for the adsorption of –OH groups arranged in such a way as to favour anatase phase formation. This assumption was corroborated by Raman, FTIR and XPS results. After immersing samples into the alkaline solution, contact angle value was very low only for the compact film, and it is believed that this is both due to the fact that such medium provides hydroxyl ions and to the compact film containing a large number of crystalline sites. This study provides new investigation perspectives aimed to improve the hydrophilic properties and biocompatibility of films through simple immersion tests. To further enrich the analysis, this monitoring can be planned in terms of minor immersion times, such as days or even hours. The inclusion of films with nanotubular morphologies, as well as nanoporous and compact films, emerges as a good strategy for such a purpose, which could be corroborated with cell viability tests planned for a further step of this investigation.

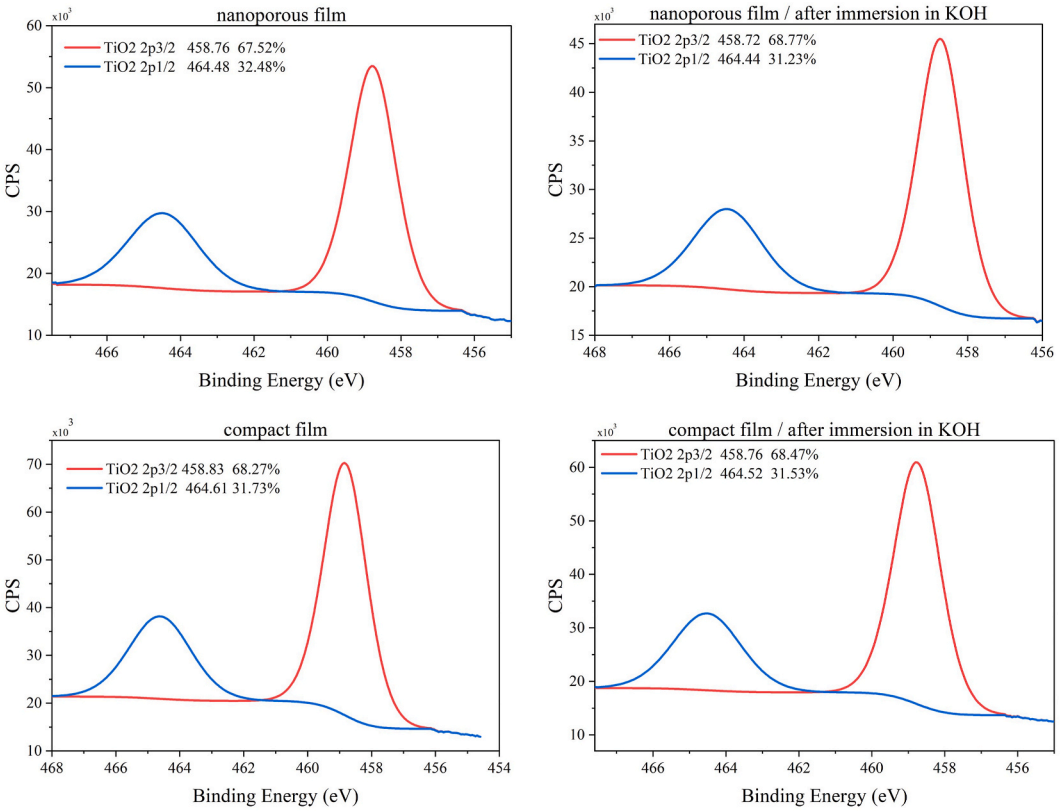

Fig. 8. (*continued*).

Data availability statement

Data included in article/supp. material/referenced in article.

CRediT authorship contribution statement

Dener Pedro da Silva Palma: Methodology, Investigation, Formal analysis, Data curation. **Giovana Pedroso Silva:** Investigation. **Fernanda Mathidios Zago:** Investigation. **Eduardo Norberto Codaro:** Writing – review & editing, Validation, Supervision. **Heloisa Andréa Acciari:** Writing – review & editing, Writing – original draft, Visualization, Supervision, Project administration, Funding acquisition, Conceptualization.

Declaration of competing interest

The authors declare that they have no known competing financial interests or personal relationships that could have appeared to influence the work reported in this paper.

Acknowledgments

To Dr. Felipe Vicente de Paula Kodaira, São Paulo State University (Unesp), School of Engineering and Sciences, Department of Physics, Guaratinguetá (FEG/Unesp) for his assistance in contact angle measurements.

To the Institutional Programs of Scientific Scholarships, PROPe-Unesp and PROPG-Unesp.

This study was partly financed by the Coordination for the Improvement of Higher Education Personnel – Brazil (Coordenação de Aperfeiçoamento de Pessoal de Nível Superior – Brasil – CAPES) – Finance Code 001.

References

[1] S. Chen, Y. Ni, J. Zhang, Y. Dan, W. Zhang, Y. Song, X. Zhu, Double-anode anodization of metal Ti in two beakers, Electrochem. Commun. 125 (2021) 106991, https://doi.org/10.1016/j.elecom.2021.106991.

[2] H. Sopha, Y. Norikawa, M. Motola, L. Hromadko, J. Rodriguez-Pereira, J. Cerny, T. Nohira, K. Yasuda, J.M. Macak, Anodization of electrodeposited titanium films towards TiO2 nanotube layers, Electrochem. Commun. 118 (2020) 106788, https://doi.org/10.1016/j.elecom.2020.106788.

[3] L. Mohan, C. Dennis, N. Padmapriya, C. Anandan, N. Rajendran, Effect of electrolyte temperature and anodization time on formation of TiO2 nanotubes for biomedical applications, mater, Today Commun. 23 (2020) 101103, https://doi.org/10.1016/j.mtcomm.2020.101103.

[4] M. Mansoorianfar, R. Rahighi, A. Hojjati-Najafabadi, C. Mei, D. Li, Amorphous/crystalline phase control of nanotubular TiO2 membranes via pressure-engineered anodizing, Mater. Des. 198 (2021) 109314, https://doi.org/10.1016/j.matdes.2020.109314.

[5] N. Pishkar, M. Ghoranneviss, Z. Ghorannevis, H. Akbari, Study of the highly ordered TiO2 nanotubes physical properties prepared with two-step anodization, Results Phys. 9 (2018) 1246–1249, https://doi.org/10.1016/j.rinp.2018.02.009.

[6] S. Wu, S. Wang, W. Liu, X. Yu, G. Wang, Z. Chang, D. Wen, Microstructure and properties of TiO2 nanotube coatings on bone plate surface fabrication by anodic oxidation, Surf. Coating. Technol. 374 (2019) 362–373, https://doi.org/10.1016/j.surfcoat.2019.06.019.

[7] D. Niu, Q. Zhou, X. Zhu, X. Feng, S. Chen, A. Wang, Y. Song, Formation of TiO2 nanopetal architectures originated from anodic titanium oxide nanotubes, Chem. Phys. Lett. 759 (2020) 137950, https://doi.org/10.1016/j.cplett.2020.137950.

[8] L. Wu, C. Li, Y. Song, K. Zhang, J. Zhang, P. Li, X. Zhu, What happens if anodic TiO2 nanotubes are soaked in H3PO4 at room temperature for a long time? Electrochem. Commun. 105 (2019) 106501 https://doi.org/10.1016/j.elecom.2019.106501.

[9] F. Yang, X. Feng, F. Ge, T. Zhang, J. Qi, D. Li, X. Zhu, Rapid growth of titanium oxide nanotubes under the critical breakdown voltage: evidence against the dissolution reaction of fluoride ions, Electrochem. Commun. 103 (2019) 17–21, https://doi.org/10.1016/j.elecom.2019.04.010.

[10] J. Zhang, W. Huang, K. Zhang, D. Li, H. Xu, X. Zhu, Bamboo shoot nanotubes with diameters increasing from top to bottom: evidence against the field-assisted dissolution equilibrium theory, Electrochem. Commun. 100 (2019) 48–51, https://doi.org/10.1016/j.elecom.2019.01.019.

[11] Z. Xu, X. Jiang, Rapid fabrication of TiO2 coatings with nanoporous composite structure and evaluation of application in artificial implants, Surf. Coating. Technol. 381 (2020) 125094, https://doi.org/10.1016/j.surfcoat.2019.125094.

[12] A. Ossowska, J.M. Olive, A. Zieliński, A. Wojtowicz, Effect of double thermal and electrochemical oxidation on titanium alloys for medical applications, Appl. Surf. Sci. 563 (2021), https://doi.org/10.1016/j.apsusc.2021.150340.

[13] N. Hu, Y. Wu, L. Xie, S.M. Yusuf, N. Gao, M.J. Starink, L. Tong, P.K. Chu, H. Wang, Enhanced interfacial adhesion and osseointegration of anodic TiO2 nanotube arrays on ultra-fine-grained titanium and underlying mechanisms, Acta Biomater. 106 (2020) 360–375, https://doi.org/10.1016/j.actbio.2020.02.009.

[14] M. Motola, R. Zazpe, L. Hromadko, J. Prikryl, V. Cicmancova, J. Rodriguez-Pereira, H. Sopha, J.M. Macak, Anodic TiO2 nanotube walls reconstructed: inner wall replaced by ALD TiO2 coating, Appl. Surf. Sci. 549 (2021), https://doi.org/10.1016/j.apsusc.2021.149306.

[15] C.M. Cotrut, I.C. Ionescu, E. Ungureanu, A. Berbecaru, R.I. Zamfir, A. Vladescu, D.M. Vranceanu, Evaluation of surface modification techniques on the ability of apatite formation and corrosion behavior in synthetic body fluid: an in vitro study, Surface. Interfac. 22 (2021) 100866, https://doi.org/10.1016/j.surfin.2020.100866.

[16] H.A. Acciari, D.P.S. Palma, E.N. Codaro, Q. Zhou, J. Wang, Y. Ling, J. Zhang, Z. Zhang, Surface modifications by both anodic oxidation and ion beam implantation on electropolished titanium substrates, Appl. Surf. Sci. 487 (2019) 1111–1120, https://doi.org/10.1016/j.apsusc.2019.05.216.

[17] D.P. Da Silva Palma, R.Z. Nakazato, E.N. Codaro, H.A. Acciari, Morphological and structural variations in anodic films grown on polished and electropolished titanium substrates, Mater. Res. 22 (2019) 1–8, https://doi.org/10.1590/1980-5373-MR-2019-0362.

[18] V. Sivaprakash, R. Narayanan, Synthesis of TiO2 nanotubes via electrochemical anodization with different water content, Mater, Today Proc. 37 (2020) 142–146, https://doi.org/10.1016/j.matpr.2020.04.657.

[19] M. Liao, H. Ma, D. Yu, H. Han, X. Xu, X. Zhu, Formation mechanism of anodic titanium oxide in mixed electrolytes, Mater. Res. Bull. 95 (2017) 539–545, https://doi.org/10.1016/j.materresbull.2017.08.041.

[20] J. Qin, Z. Cao, H. Li, Z. Su, Formation of anodic TiO2 nanotube arrays with ultra-small pore size, Surf. Coating. Technol. 405 (2021) 126661, https://doi.org/10.1016/j.surfcoat.2020.126661.

[21] Q. Zhou, M. Tian, Z. Ying, Y. Dan, F. Tang, J. Zhang, J. Zhu, X. Zhu, Dense films formed during Ti anodization in NH4F electrolyte: evidence against the field-assisted dissolution reactions of fluoride ions, Electrochem. Commun. 111 (2020) 106663, https://doi.org/10.1016/j.elecom.2020.106663.

[22] G. Wang, Y. Wan, B. Ren, Z. Liu, Bioactivity of micropatterned TiO 2 nanotubes fabricated by micro-milling and anodic oxidation, Mater. Sci. Eng. C 95 (2019) 114–121, https://doi.org/10.1016/j.msec.2018.10.068.

[23] S. Durdu, G. Cihan, E. Yalcin, A. Altinkok, Characterization and mechanical properties of TiO2 nanotubes formed on titanium by anodic oxidation, Ceram. Int. 47 (2021) 10972–10979, https://doi.org/10.1016/j.ceramint.2020.12.218.

[24] A. Aeimbhu, Effect of calcination temperature on morphology, wettability and anatase/rutile phase ratio of titanium dioxide nanotube arrays, Mater. Today Proc. 5 (2018) 14950–14954, https://doi.org/10.1016/j.matpr.2018.04.036.

[25] P. Agilan, K. Saranya, N. Rajendran, Bio-inspired polydopamine incorporated titania nanotube arrays for biomedical applications, Colloids Surfaces A Physicochem. Eng. Asp. 629 (2021) 127489, https://doi.org/10.1016/j.colsurfa.2021.127489.

[26] N. Arsalani, Y. Panahian, R. Nasiri, Fabrication of novel magnetic F-TiO2(B)/carbon nanostructures nanocomposites as photocatalysts for malachite green degradation under visible light, Mater. Sci. Eng. B Solid-State Mater. Adv. Technol. 251 (2019) 114448, https://doi.org/10.1016/j.mseb.2019.114448.

[27] A. Zarebidaki, S.H.H. Mofidi, A.S. Nodezh, Corrosion mechanism of titanium dioxide nanotubes in Ringer's solution, Mater. Today Commun. 29 (2021) 102943, https://doi.org/10.1016/j.mtcomm.2021.102943.

[28] V. Mandić, I. Panžić, M. Kraljić-Roković, M. Gaboardi, Breakdown of the anodized nanostructured anatase for photovoltaic devices: the effect of water content in the electrolyte on preparation of large surfaces of nanotubes, Ceram. Int. 49 (2023) 14844–14854, https://doi.org/10.1016/j.ceramint.2022.07.254.

[29] Y. Shen, C. Xie, X. Xiao, Black phosphorus-incorporated titanium dioxide nanotube arrays for near-infrared–triggered drug delivery, J. Drug Deliv. Sci. Technol. 72 (2022) 103400, https://doi.org/10.1016/j.jddst.2022.103400.

[30] X. Wang, D. Zhang, Q. Xiang, Z. Zhong, Y. Liao, Review of water-assisted crystallization for TiO2 nanotubes, Nano-Micro Lett. 10 (2018) 1–28, https://doi.org/10.1007/s40820-018-0230-4.

[31] M. Benčina, A. Iglič, M. Mozetič, I. Junkar, Crystallized tio2 nanosurfaces in biomedical applications, Nanomaterials 10 (2020), https://doi.org/10.3390/nano10061121.

[32] D. Regonini, C.R. Bowen, A. Jaroenworaluck, R. Stevens, A review of growth mechanism, structure and crystallinity of anodized TiO2 nanotubes, Mater. Sci. Eng. R Rep. 74 (2013) 377–406, https://doi.org/10.1016/j.mser.2013.10.001.